Archetypal energy landscapes: Dynamical diagnosis

Florin Despa
Department of Chemistry, University of Chicago, Chicago, Illinois 60637

David J. Wales
University Chemical Laboratories, Lensfield Road, Cambridge CB2 1EW, United Kingdom

R. Stephen Berry
Department of Chemistry, University of Chicago, Chicago, Illinois 60637

(Received 23 June 2004; accepted 15 October 2004; published online 17 December 2004)

Recent studies have identified several motifs for potential energy surfaces corresponding to distinct dynamic and thermodynamic properties. The corresponding disconnectivity graphs were identified as ''palm tree,'' ''willow tree,'' and ''banyan tree'' patterns. In the present contribution we present a quantitative analysis of the relation between the topography and dynamics for each of these motifs. For the palm tree and willow tree forms we find that the arrangement of the stationary points in the monotonic sequences with respect to the global minimum is the most important factor in establishing the kinetic properties. However, the results are somewhat different for motifs involving a rough surface with several deep basins (banyan tree motif), with large barriers relative to the energy differences between minima. Here it is the size of the barrier for escape from the region relative to the barriers at the bottom that is most important. The present results may be helpful in distinguishing between the dynamics of ''structure seeking'' and ''glass forming'' systems.
 [DOI: 10.1063/1.1829633]

I. INTRODUCTION

The underlying potential energy surface (PES) of a molecular system ultimately determines its structure, dynamics, and thermodynamics.[1] Coarse graining the PES into a disjoint regions of configuration space can be particularly insightful: partition functions can be written as a superposition sum over contributions from different regions, while dynamics can be treated in terms of transitions between regions.[1–6] The most commonly used approach is to partition the configuration space into the catchment basins, or basins of attraction, and then to express the dynamics in terms of transitions between local minima.[1–4] Methods based upon master equation dynamics,[7,8] kinetic Monte Carlo schemes,[9–11] discrete path sampling,[1,12] and characteristic escape rates[6] have all been considered.[1–4] Various grouping schemes for local minima have also been employed to simplify such kinetic schemes and avoid numerical problems in master equation calculations.[13–15] Such strategies seem very informative in the study of dynamics of conformationally constrained systems, where the constriction in the conformation space may frequently culminate with splitting of the energy landscape into multiple competing basins.[16] This approach also helps us to understand kinetic traps in a more quantitative manner,[17] as well as competing reactive pathways.[18]

Visualizing the topology of a multidimensional PES provides a helpful first step in explaining how observed properties are determined by the surface. Two approaches have mainly been employed for this purpose, namely, monotonic sequences[2,3] of local minima with decreasing potential energy (and the intervening transition states), which reveal local and regional topography of the landscape, and disconnectivity graphs,[5] which emphasize the global topology. The information required for both constructions consists of a database of local minima and the transition states that connect them. Naturally, for systems of many particles, one can expect to work only with a statistical sample of the stationary points.

In a disconnectivity graph analysis, the minima are classified into disjoint sets (or ''superbasins''[5]) at a series of energies E_i. Two minima are in the same set at energy E_i if they can be interconverted without exceeding this threshold energy. Each set is represented by a node on the horizontal axis at energy E_i, and nodes are joined by upward lines if the corresponding basins merge together at the higher energy E_{i+1}. Each local minimum is represented as a single node or lower terminus at a height on the vertical axis corresponding to its potential energy; these nodes are then joined together by upward lines as they merge into superbasins with increasing energy. The vertices at which upward lines meet indicate the energy bands of connecting saddles, the bands in which a system can pass by classical motion between the minima linked at each vertex.

Three archetypal motifs have been identified in disconnectivity graphs for molecular systems, and may be recognized as ''palm tree,'' ''willow tree,'' and ''banyan tree'' patterns.[1,19] The first two motifs can both be described in terms of monotonic sequences leading to the global potential energy minimum. They are distinguished because for the palm tree the downhill barriers are smaller than the separations between successive minima, while for the willow tree they are large (Figs. 1 and 2). In both cases cutting a single edge of the graph disconnects a single minimum. The banyan tree considered in earlier work[5,19] is qualitatively different,

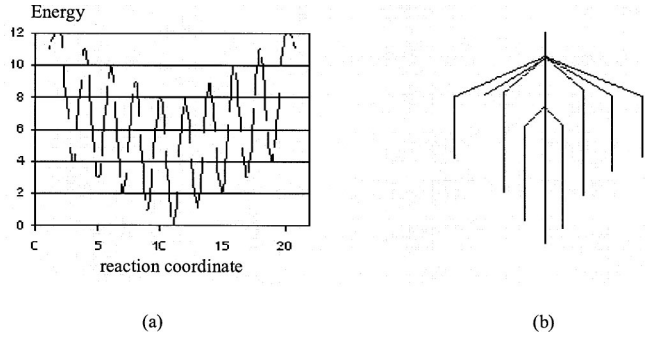

FIG. 1. (a) A potential energy surface with large barriers compared to the energy differences between successive local minima. (b) The resulting ''weeping willow'' disconnectivity graph.

since barrier heights on different energy scales lead to a hierarchical structure, where cutting a single edge can disconnect a whole subset of local minima [Figs. 3(b) and 3(c)]. The energy barriers are also large compared to the energetic separation of the local minima, and there is no well-defined global minimum. Thus the banyan tree motif is associated with landscapes with several (or many) deep basins, as exemplified by a model $(H_2O)_{20}$ cluster.[19] The multiple funnel landscapes of alkali halide clusters[20,21] and the BLN model protein[22–24,13] can also be viewed in this way. In the present work we consider a simple version of the banyan motif with a single barrier height and local minima of identical energy. This topology does not have the hierarchical structure of the original model, but still displays a highly degenerate lowest energy minimum [Fig. 3(a)]. For each landscape we define one larger barrier, which delimits the set of local minima and enables us to define an escape time for the region as a whole.

The main aim of the present work is to characterize the dynamics associated with each of the classes of landscapes described by the disconnectivity graphs described above. In particular, we will investigate how the average escape time from the set of local minima associated with each motif depends upon characteristic energy scales, such as barrier heights, and upon length scales characterited by the number of local minima along a pathway. The calculated escape rates allow us to quantify and compare kinetic properties for such regions, and can be used to investigate dynamics of more complex landscapes composed of combinations of such

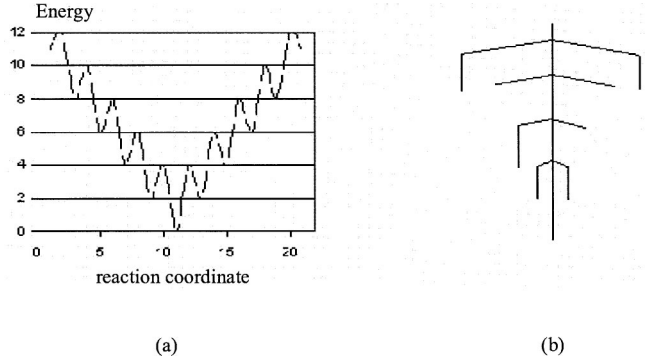

FIG. 2. (a) A potential energy surface with small barriers compared to the energy differences between successive local minima. (b) The resulting ''palm tree'' disconnectivity graph.

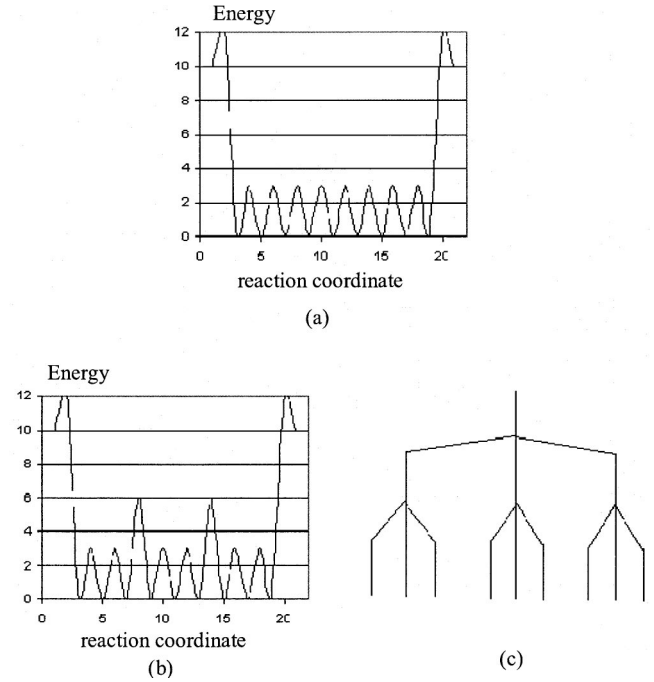

FIG. 3. (a) A potential energy surface consisting of degenerate local minima. (b) Combining two such surfaces with different barrier heights produces the characteristic ''banyan tree'' pattern with a hierarchical structure in the disconnectivity graph (c).

structures. In addition, we study the kinetic properties of each of these classes of landscapes for both low and intermediate friction regimes. The former corresponds to a situation of an energy-controlled reaction with the kinetic rate depending on the coupling of the reaction coordinate to the thermal bath.[6] This is the case where the reaction coordinate is the energy of a molecular vibrational coordinate.[18] The latter represents the case in which the reaction rate is insensitive to the coupling with the thermal bath and is known as the transition state theory (TST) regime. The high friction regime, where the reaction can be viewed as a spatial diffusion, is especially relevant for chemical reactions in condensed phases, surface desorption and diffusion of atoms or ions in solids. There is an increasing indication that this regime can be relevant for describing protein folding kinetics in solutions (see, for example, the work by Plaxco and Baker[25]). This aspect is the subject of a forthcoming paper.

II. MODEL POTENTIAL ENERGY LANDSCAPES

To facilitate a proper comparison of the kinetics, we now consider three model potential surfaces with the same number of stationary points in the region of interest, i.e., nine minima and ten saddles. The one-dimensional surfaces are illustrated in Figs. 1(a), 2(a), and 3(a), where the horizontal coordinate corresponds to the integrated path length. The energy of the highest two transition states, corresponding to escape from each region, is defined as E_D, relative to the global minimum in each case.[26,27] For every canonical simulation we set $E_D = 12k_BT$, where T is the temperature. The energy difference between successive minima is defined as ΔE, and, in the model used here, this is also the difference between uphill and downhill barriers for each minimum:

$$\Delta E = |E_i - E_{i+1}|. \tag{2.1}$$

The surfaces illustrated in Figs. 1(a), 2(a), and 3(a) correspond to $\Delta E = k_B T$, $\Delta E = 2k_B T$, and $\Delta E = 0$, respectively.

III. THE ESCAPE RATE FROM A REGION

We consider two methods for quantifying and comparing the dynamics corresponding to the landscapes defined in Sec. II, the interbasin motion (IBM) and master equation (ME) approaches. The IBM approach is appropriate to study the energy diffusion regime in the case of low coupling of the system with the thermal bath. This introduces in the system's dynamics features of the contact between the system and the thermal bath through a memory function. The ME approach with the corresponding TST rates is employed to investigate the case of an ideal contact of the system with the thermal bath in which the kinetic rates do not depend on the properties of the thermal bath. In the limit when the memory friction parameter tends to zero, the two approaches yield similar results, as we have shown recently.[28]

A. Interbasin motion approach

The principal assumption of the IBM approach is that the dynamics for transitions between local minima within a region are much faster than the rate of escape over the highest transition state. In some situations the internal time scale characterizing transitions of the system of interest is shorter than that for thermalizing with the surrounding bath.[29] The dynamics within a region may then become non-Markovian. This behavior can be modeled by a time-dependent friction kernel $Z(t)$, which represents contact between the system and the thermal bath, and is assumed to have a Gaussian form[29]

$$Z(t) = \frac{\gamma}{\tau_c \sqrt{\pi}} \exp\left(- \frac{t^2}{4t_c^2} \right). \tag{3.1}$$

$Z(t)$ expresses the time correlation function of the random force $F(t)$ exerted by the thermal bath on the reactive mode, and is associated with the correlation time t_c and the Markovian friction γ. t_c is a measure of the time required for equipartition of energy between the reaction coordinate and the thermal bath. The random force $F(t)$ exerted by the thermal bath on the reaction coordinate is also assumed to be Gaussian and satisfies the second fluctuation dissipation theorem

$$\langle F(t)F(0) \rangle = M k_B T Z(t), \tag{3.2}$$

where M is the mass of the system.

The above framework provides a connection to the probability distribution for the energy associated with the reaction coordinate E:

$$\frac{\partial p}{\partial t} = \frac{\partial}{\partial E} \left[\mu(E) \left(\frac{\partial}{\partial E} + \frac{1}{k_B T} \right) \omega(E) p(E,t) \right], \tag{3.3}$$

where μ is the energy diffusion coefficient and $\omega(E)$ is the frequency, which depends on the local curvature of the PES determined by the effective potential function. Equation (3.3) is known as the reduced Fokker-Planck equation, which gives the probability distribution $p(E,t)$ for E. It is generally considered to be equivalent to the phenomenological Langevin equation.[30] A steady state solution of Eq. (3.3) exists with the form

$$p_{ss}(E) = F(E) \exp\left(- \frac{E}{k_B T} \right), \tag{3.4}$$

where $F(E)$ is the "correction function".[31]

Using the above steady-state solution one defines a mean time

$$\tau(E,E_s) = \int_{E_s}^{E} \int_0^{E''} \frac{\exp(\beta E'')}{\mu(E'')} \frac{\exp(-\beta E')}{\omega(E')} dE'\, dE'' \tag{3.5}$$

required for the system to reach energy E starting from a point E_s in a potential well at $t=0$, where $\beta = 1/k_B T$. The escape rate from a local minimum is defined as the average of the mean first passage time $\tau(E,E_s)$ over the steady state distribution p_{ss}.[32] For a region containing more than one local minimum, we define an effective mean first passage time $\tau_{\text{eff}}(E_D,E_s)$, which accounts for the entire distribution of "escape channels" that carry the system over the highest transition states at energy E_D. We then use the following equation for computing the escape rate from such a region:

$$k = \int_0^{E_D} \frac{p_{ss}(E_s)}{\tau_{\text{eff}}(E_s,E_D)} dE_s. \tag{3.6}$$

B. Master equation approach

For Markovian systems, standard statistical rate methods, such as TST, can be used to calculate rate constants for all the individual transitions between adjacent local minima. One thing needs to be discussed at this point. The TST theory is insensitive to the coupling with the thermal bath. However, the TST theory can give a good account of the rate constant under conditions if the friction is sufficiently high to provide a continual equilibrium distribution of the reactive high energy modes, but remains sufficiently weak so that reactive barrier passage is unperturbed.[29] This is an intermediate friction regime, which differs both from the high friction regime, where the reaction can be viewed as a spatial diffusion, and from the low friction domain of the energy-controlled reaction that was discussed above.

The resulting coupled first-order differential equations for the occupation probabilities of all the local minima constitute the ME:[7,8]

$$\frac{dP_i(t)}{dt} = \sum_j w_{ij} P_j(t), \tag{3.7}$$

where $w_{ij} = W_{ij} - \delta_{ij} \Sigma_k W_{kj}$ and W_{ij} is the transition rate from minimum i to minimum j. $P_i(t)$ gives the probability of the system being in local minimum i at time t. The resulting matrix formulation may be solved by diagonalization or numerical propagation to obtain the time-dependent occupation probabilities for the individual minima and the region as a whole. We can use either microcanonical or canonical rates and in the harmonic TST approximation the corresponding matrix elements are

$$W_{ij}=\begin{cases}\dfrac{\overline{\nu_i^n}}{\overline{\nu_{ij}^{n-1}}}\left(\dfrac{E-E_{ij}}{E-E_i}\right)^{n-1} & \text{(microcanonical)}\\ \dfrac{\overline{\nu_i^n}}{\overline{\nu_{ij}^{n-1}}}\exp(-\beta E_{ij}) & \text{(canonical)},\end{cases} \tag{3.8}$$

where E_i is the potential energy of local minimum i with geometric mean vibrational frequency $\overline{\nu_i}$, E_{ij} is the energy of the transition state that connects minima i and j with geometric mean vibrational frequency $\overline{\nu_{ij}}$, and n is the number of vibrational degrees of freedom. The above formulas assume that all the minima have C_1 symmetry and that there are no degenerate rearrangements.[1] We further assume that the mean vibrational frequency varies as $\overline{\nu_i}=1-(m-1)\Delta\nu$, where m is the number of steps required to reach the global minimum. $\overline{\nu_i}$ therefore decreases linearly with increasing potential energy. We choose the unit of time as the mean vibrational period of the global minimum. $\overline{\nu_{ij}}$ is further assumed to be the geometric mean of the vibrational frequencies of the two adjacent minima that the corresponding transition state connects, i.e., $\overline{\nu_{ij}}=\sqrt{\overline{\nu_i}\overline{\nu_j}}$.

We include a backward transition rate W_b for probability of transfer back into the region over the highest transition states, and set $W_b=2k_BT$. The dynamics were then solved numerically for an initial condition where the system resides in the global minimum, i.e., $P_1(0)=1$. We denote the equilibrium occupation probability for individual local minima and for the region as a whole by $P_i^{(eq)}$ and $P_\alpha^{(eq)}=\Sigma_i^N P_i^{(eq)}$, respectively. Here the subscript α is used to distinguish the different model landscapes: $\alpha=p$, w, and b for the palm tree, willow tree, and banyan tree, respectively. The time-dependent occupation probability for each region is simply defined as $P_\alpha(t)=\Sigma_i^N P_i(t)$. Using detailed balance we obtain the effective escape rate from a region as

$$W_\alpha^{(\mathrm{eff})}=W_b\frac{P_\alpha^{(out)}}{P_\alpha^{(eq)}}=W_b\sum_i^N\frac{P_i^{(eq)}}{P_\alpha}, \tag{3.9}$$

where $P_\alpha^{(out)}$ is the total probability located outside the basin so that $P_\alpha^{(out)}(t)=1-P_\alpha(t)$.

IV. RESULTS

A. The palm and willow tree motifs

Both the palm and willow tree patterns correspond to landscapes with a systematic potential energy bias towards the global minimum (Figs. 1 and 2). We begin by applying the IBM approach and assume that all the individual local minima $i\in 1,2,...,N$ contribute independently to the effective value of the mean first passage time $\tau_{\mathrm{eff}}(E_s,E_D)$ according to the phenomenological estimate

$$\frac{1}{\tau_{\mathrm{eff}}(E_s,E_D)}=\sum_{i<j}^{N=9}\frac{f_{ij}}{\tau_{ij}(E_s,E_{ij})}. \tag{4.1}$$

Here, f_{ij} is the weight of each individual contribution to the average (4.1) given by

$$f_{ij}=\vartheta(E_{ij}-E_s)\,\vartheta(E_s-E_i), \tag{4.2}$$

where ϑ is the unit step function; E_i and E_{ij} are again the energies of local minimum i and of the transition state connecting minima i and j. τ_{eff} is the average time required for the system to reach energy E_D (the highest transition states) starting from energy E_i (at the bottom of a particular local well).

We now need to compute all the contributions τ_{ij} to the average (4.1). The mean first passage time[32] along each escape channel is defined in the framework of non-Markovian dynamics theory by

$$\tau_{ij}(E_s,E_{ij})=\int_{E_s}^{E_{ij}}\int_0^E\frac{\exp(\beta E)}{\mu_{ij}(E)}\frac{\exp(-\beta E')}{\omega_{ij}(E')}dE\,dE'. \tag{4.3}$$

Equation (4.3) contains all the requisite information about the main properties of the PES topography, particularly the relative positions of minima and transition states along the monotonic sequences. In addition, general properties of the thermal bath are included in the dynamics through the mean energy diffusion coefficient $\mu_{ij}(E)$. Here we approximate μ by a harmonic oscillator of frequency $\omega_{ij}(E)=\omega_0$. The corresponding energy diffusion coefficient is then[29]

$$\mu(E)=\frac{E\gamma}{\beta\omega_0}\exp(-\rho^2), \tag{4.4}$$

where $\rho=\omega_0 t_c$ determines the memory friction parameter. In the present work we have set $\rho=0.3$, which is in the low friction regime,[29] and assume a steady state distribution of Boltzmann form for p_{ss}:

$$p_{ss}(E_s)=A_0e^{-\beta E_s}, \tag{4.5}$$

where A_0 is a normalization constant.

The parameter γ depends on the viscosity of the environment and on the characteristic geometry of the system inside the region in question. Hence, we may write down the following approximation $\gamma_\zeta\simeq\pi\langle R\rangle_\zeta\eta n/M$, where $\langle R\rangle_\zeta$ is the radius of gyration of the system averaged over the conformations in the region ζ, η is the viscosity, and n is an integer depending on the (slip or stick) boundary condition at the interface. On the other hand, the frictional relaxation time t_c and the Markovian friction constant γ are related by $t_c=a\gamma$, where a is essentially the inverse of the infinite frequency shear modulus of the solvent. In this context, we may determine the corresponding friction correlation time $t_{c\zeta}$ and damping rate γ_ζ for each region on the PES. This result implies that the relaxation behavior depends intrinsically on the way the various conformations of the system couple to the thermal bath.[28]

We now use Eqs. (3.6) and (4.1)–(4.5) to compute the escape rate k for regions corresponding to the palm tree and willow tree motifs within the IBM model. The numerical value of the escape rate for the willow tree region is $k_w=0.48\times10^{-2}$ in units of $\gamma\,(\sim10^{13}\,\mathrm{s}^{-1})$, while for the palm tree the corresponding result is $k_p=0.8\times10^{-1}$. (All the numerical results for the escape rates are given in units of the damping rate γ.) We see that the rate is more than one order of magnitude higher for the palm tree with $k_p/k_w=16.7$. Hence, for regions with the same depth, the rate of escape is larger for the palm tree topology because the intervening

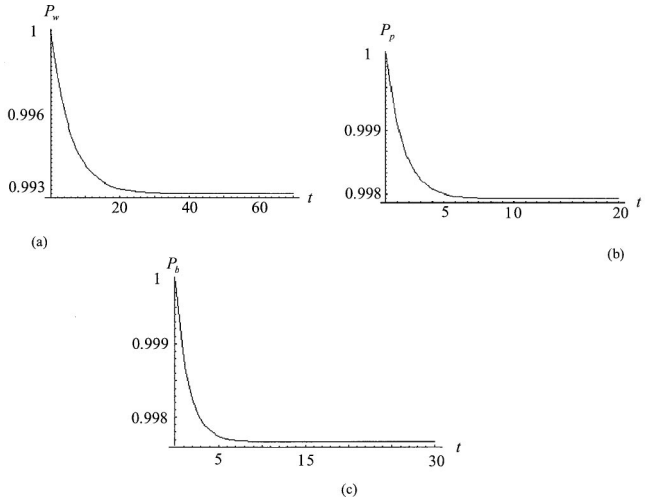

FIG. 4. The time evolution of the canonical probability densities $P_\alpha(t)$ for the willow tree (a), palm tree (b), and banyan tree (c) landscapes.

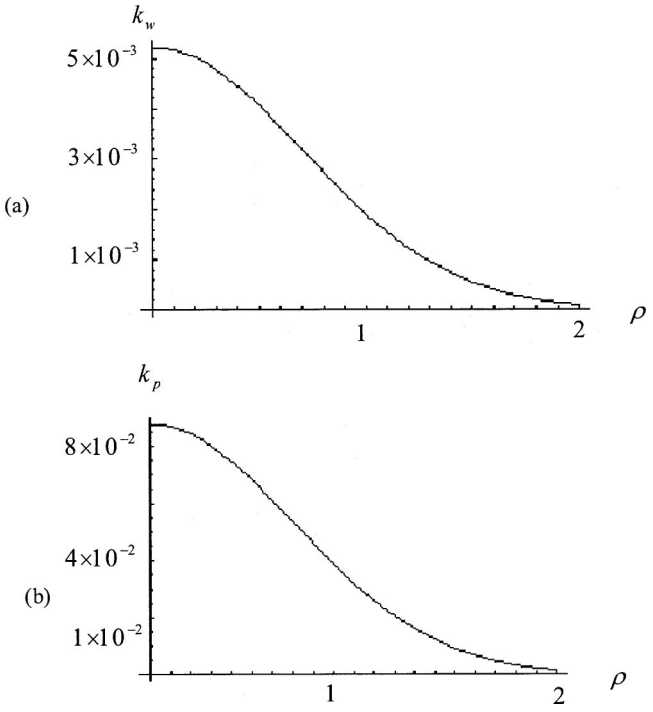

FIG. 5. The relation between thermal bath properties and dynamics: escape rate as a function of the memory friction parameter ρ for the willow tree (a) and palm tree (b) landscapes.

barriers are smaller. However, there is one less obvious observation to be made. If the escape rate is calculated for a smooth potential well of the same depth ($12k_BT$) we obtain a value of 0.6×10^{-4}, which is much smaller than both k_p and k_w. A higher density of local minima along the way out of a large basin can be expected to increase the escape rate.[6]

When studying model landscapes it is important to realize that some of the parameters in question may actually be correlated in real systems. For example, ''strong'' and ''fragile'' characteristics[33–35] in thermodynamic and dynamic properties can be varied independently in models.[36–41] However, the correlation can be recovered if we recognize that a higher density of local minima in configuration space would presumably necessitate higher curvatures and hence vibrational frequencies.[38] ''Fragile'' behavior is then associated with more local minima and higher frequencies,[33] and may result in non-Arrhenius temperature dependence for diffusion and a large heat capacity peak at the glass transition.[38]

Turning now to the master equation approach in Sec. III B we evaluate $W_p^{(\mathrm{eff})}/W_w^{(\mathrm{eff})}$. The parameters employed in the present computation are $k=101$ and $\Delta\nu=0.01$. The energies of the local minima and transition states were the same as for the IBM calculations described above, and in the microcanonical ensemble the total energy was set at $E=60$. However, very similar results were obtained for the microcanonical and canonical ensembles, so only the canonical results will be described here. The time evolution of the occupation probabilities, $P_\alpha=\Sigma_i^N P_i(t)$, $\alpha=p$, w, is shown in Figs. 4(a) and 4(b). The asymptotic value of P_w is larger by about a factor of 5.5 and the equilibrium probability density is higher for the willow tree pattern.

Using Eq. (3.9) we have derived the equilibrium probability densities $P_p^{(eq)}$ and $P_w^{(eq)}$ and then estimated $W_p^{(\mathrm{eff})}/W_w^{(\mathrm{eff})}$, which is $W_p^{(\mathrm{eff})}/W_w^{(\mathrm{eff})}\simeq5.6$, a result qualitatively similar to that obtained above. In the limit $\rho\to0$, which is characteristic of ideal Markovian behavior, the ratio k_p/k_w achieves values comparable to $W_p^{(\mathrm{eff})}/W_w^{(\mathrm{eff})}$, as can be inferred from Fig. 5.

The IBM and ME approaches lead to similar conclusions with respect to the dynamics within the two regions. The change in barrier heights obtained by tuning ΔE from k_BT to $2k_BT$ leads to a significant increase in the escape rate, as well as the relaxation rate considered in previous work.[1,42,43,20,44]

B. The banyan tree motif

The model PES shown in Fig. 3(a) simply involves a periodic potential within the region in question, with higher barriers for escape. Similar surfaces with fewer local minima have previously been considered for internal rotation.[45] The corresponding Hamiltonian is then

$$H=\frac{p^2}{2I}-U_0\cos x, \tag{4.6}$$

where I is the moment of inertia of the rotating group, x is the reaction coordinate, and $U_0=E_d/2$, with E_d the amplitude of the oscillations [see Fig. 3(a)]. The appropriate frequency and energy diffusion coefficient for such a PES are[46,47]

$$\omega_1=\omega_0\pi\frac{1}{2\mathcal{K}(\epsilon)},$$
$$\mu_1=\frac{4\gamma E_d}{\pi\beta\omega_0}\exp(-\omega_l t_c)^2[\mathcal{E}(\epsilon)-(1-\epsilon)\mathcal{K}(\epsilon)] \tag{4.7}$$

for $E<E_d$ and

$$\omega_2 = \omega_0 \pi \frac{\sqrt{\epsilon}}{\ln\left(\frac{16E}{E-E_d}\right)},$$
$$\mu_2 = \frac{4\gamma E}{\pi\beta\omega_0}\exp(-\omega_u t_c)^2 \mathcal{E}(\epsilon^{-1}), \tag{4.8}$$

otherwise. The subscripts 1 and 2 refer here to the two distinct energy domains $E<E_d$ and $E\geqslant E_d$. Here ω_0 is the harmonic frequency, $\epsilon=E/E_d$, and $\mathcal{K}(\epsilon)$ and $\mathcal{E}(\epsilon)$ are complete elliptic integrals of the first and second kind, respectively.[48]

For this PES the effective mean first passage time $\tau_{\text{eff}}^{(b)}$ is

$$\tau_{\text{eff}}^{(b)}(E_s,E_D) = \int_{E_s}^{E_D}\int_0^E \frac{\exp(\beta E)}{\mu_2(E)}\frac{\exp(-\beta E')}{\omega_2(E')}dE'\,dE. \tag{4.9}$$

To calculate the escape rate k_b we need to evaluate the correction function $F(E)$, which appears in Eq. (3.4). Using Eqs. (3.3) and (3.4), we obtain for $F(E)$ the particular solutions

$$F_1(E) = A_1 + B_1\int_0^E \frac{1}{\mu_1(E)}\exp\left(\frac{E'}{k_BT}\right)dE', \quad E<E_d,$$
$$F_2(E) = A_2 + B_2\int_{E_d}^E \frac{1}{\mu_2(E)}\exp\left(\frac{E'}{k_BT}\right)dE', \quad E\geqslant E_d, \tag{4.10}$$

which lead to

$$p_{ss,1} = F_1(E)\exp(-\beta E_s), \quad E<E_d,$$
$$p_{ss,2} = F_2(E)\exp(-\beta E_s), \quad E\geqslant E_d. \tag{4.11}$$

By imposing in Eq. (4.10) the limit $F_2(E)\to 0$ for $E\to\infty$, we obtain

$$A_2 = -B_2\int_{E_d}^{\infty}\frac{1}{\mu_2(E)}\exp\left(\frac{E'}{k_BT}\right)dE'. \tag{4.12}$$

The remaining constants A_1, B_1, and B_2 are determined from the continuity requirements

$$j_1(E_d) = j_2(E_d),$$
$$p_{ss,1}(E_d) = p_{ss,2}(E_d), \tag{4.13}$$

and from the normalization condition

$$\int_0^{E_D} p_{ss}(E_s)dE_s = 1. \tag{4.14}$$

The first condition in Eq. (4.13) represents the continuity of the steady state flow

$$j = -\mu(E)\left[\frac{dp_{ss}}{dE} + \beta p_{ss}\right] \tag{4.15}$$

at the energy threshold E_d, while the second condition describes the continuity of the probability distribution at the same point. Under such circumstances the escape rate is

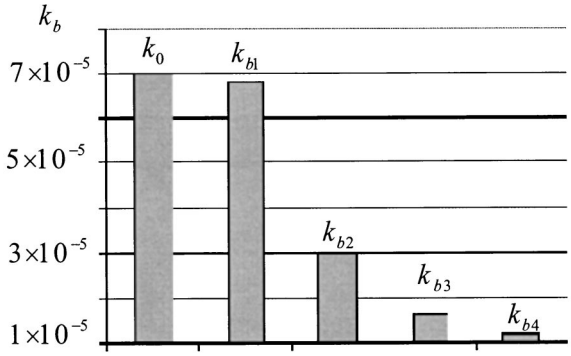

FIG. 6. Escape rates from the banyan tree type landscape for different values of the energy threshold E_d.

$$k_b = \int_{E_d}^{E_D}\frac{p_{ss,2}(E_s)}{\tau_{\text{eff}}^{(b)}(E_s,E_D)}dE_s, \tag{4.16}$$

where $\tau_{\text{eff}}^{(b)}$ given by Eq. (4.9). All the constants needed for computing escape rates from the landscapes illustrated in Figs. 3(a) and 3(b) are derived in the Appendix.

In Fig. 6, we display values of the escape rates $k_b(E_d)$ with threshold energies E_d ranging between k_BT and $4k_BT$. Generally, the escape rate decreases as the amplitude of the oscillations increases. Obviously, as E_d tends to zero the escape rate should tend to the value corresponding to a single smooth potential well, k_0. As we can see from Fig. 6, k_b does indeed tend to k_0 as E_d decreases.

Combining two periodic-type surfaces with different barrier heights produces a hierarchical landscape of the kind originally associated with a banyan tree[42] [Fig. 3(b)]. The escape rate for such a region could be calculated in the same manner as above.

We now turn to the master equation approach (Sec. III B) and apply this method to the model PES shown in Fig. 3(a). It can be seen from Fig. 4(c) that the total occupation probability P_b for this motif achieves a high value, which corresponds to a low escape rate. The $P_b(t)$ plot shown in Fig. 4(c) was obtained for $E_d=2k_BT$. On increasing these potential barriers, the equilibration inside the basin slows down. For example, we found that the equilibration time is $t_e=11$ in units of the vibrational period for potential barriers of $2k_BT$, which increases to $t_e=42$ for $E_d=3k_BT$.

We performed a similar analysis of the banyan tree motif for the microcanonical ensemble. All common parameters were fixed at the same values as above, and the total energy was set to $E=60$. In contrast to the results of Sec. IV A, we found that the transition rates were all much smaller than for the canonical simulation. The equilibration time also increased; for example, we found $t_e=20$ for barriers of $2k_BT$ and $t_e=110$ for $E_d=3k_BT$. As a general observation we found that the microcanonical equilibrium value of $P_b^{(eq)}$ did not change significantly with E_d.

V. CONCLUSIONS

We have investigated and compared the escape rates from potential energy surfaces with characteristic palm tree, willow tree, and banyan tree topologies. One important result is that the escape rates are sensitive to the relative positions of stationary points on the monotonic sequences that lead to the global minimum. In addition, the rates k_p and k_w for the palm tree and willow tree motifs are always greater than the rate for a smooth potential well with the same overall depth E_D, consistent with earlier results.[6] Hence the presence of local minima increases the escape rate. For landscapes corresponding to the banyan tree pattern, the ratio between the depth of the region E_D and the amplitude of the barriers between local minima E_d primarily determines the escape rate (Fig. 6). These observations may be useful in future comparisons of ''structure seeking'' and ''glassy'' landscapes.[49]

Both IBM and ME approaches led to similar conclusions with respect to the dynamics within the regions of palm tree and willow tree motifs. The change in barrier heights obtained by tuning ΔE from k_BT to $2k_BT$ leads to a significant increase in the escape rate from that region. However, the quality of the contact with the thermal bath (the value of the memory function parameter) leads to important variations of the kinetic rates, a fact that can be inferred from Fig. 5. In the limit when the memory friction parameter tends to zero, the ratio k_p/k_w (IBM approach) achieves values comparable to $W_p^{(\mathrm{eff})}/W_w^{(\mathrm{eff})}$ (ME approach). Otherwise, the dynamics corresponding to the two energy surface archetypes is dependent on the solvent model. This result suggests that the solvent might be an important factor in setting the kinetic properties of the effective energy landscape, as suggested recently.[50]

The inverse of the escape rate $1/k$ is the average residence time within the corresponding region of the PES, τ^*. Such lifetimes may be of interest in analyzing questions such as the bioactivity of proteins, where the escape rates from different configurations can be dictated by the vibrational energy transfer. It has been also suggested that the rate of aggregation of unfolded proteins may depend on the lifetime of the unfolded state τ_u^*,[51] as well as the relative populations in the native and unfolded states. The larger the value of τ_u^*, the higher is the probability that the unfolded protein will aggregate with other unfolded proteins. The lifetime of the unfolded state of the protein involves nascent vibrationally excited states that have difficulty becoming energetically stabilized. The IBM approach seems suitable to address such a question and provides a means to calculate average lifetimes for specific regions of configuration space.

The high friction regime, which was not discussed here, can be seen as a spatial diffusion.[52,53] This is mostly relevant for chemical reactions in condensed phases, surface desorption, and diffusion of atoms or ions in solids. It has been shown, for example, that the spatial diffusion can be drastically affected by the presence of the intervening minima.[54] The increase in the spatial diffusion depends on the degree of geometrical degeneracy of the off-center potential. This explains why diffusion coefficients of off-center impurities are usually larger than diffusion coefficients of on-center impurities.[54]

There is increasing indication that the high friction regime can be relevant for describing protein folding kinetics in solutions (see, for example, the work by Plaxco and Baker[25]). This aspect is the subject of a forthcoming paper.

Finally we note that the treatment of dynamics via coarse graining into transitions between local minima has several important advantages over direct simulation. Some are matters of practicability. Obtaining interbasin transition rates using the corresponding transition states offers a way to speed up the computation and to reduce the dimension of the system of kinetic equations without losing information about the topography and configuration entropy. Such methods can be used to infer kinetic properties for relatively large regions of the PES quite efficiently.[1,12,14,16,43,55,56] Coarse graining in this way can also provide a more compact and insightful description of the phenomenon of interest. An example is the issue of estimating the effect of mutations on structure and overall dynamics:[57–60] Previous work[16] suggests that it is more relevant in this case to focus on the ability of the system to survey well-defined basin, rather than monitoring single state occupancies.

APPENDIX: THE PROBABILITY DISTRIBUTION FOR A PES WITH A CHARACTERISTIC BANYAN TREE TOPOLOGY

Here we provide the constants entering the equation for the steady state probability distribution

$$p_{ss}(E)=\begin{cases}\left(B_1+A_1\int_0^E dE'\dfrac{\exp(\beta E')}{\mu_1(E')}\right)\exp(-\beta E) & (E<E_1)\\ \left(B_2+A_2\int_{E_1}^E dE'\dfrac{\exp(\beta E')}{\mu_2(E')}\right)\exp(-\beta E) & (E_1\leqslant E\leqslant E_2)\\ \left(B_3+A_3\int_{E_2}^E dE'\dfrac{\exp(\beta E')}{\mu_3(E')}\right)\exp(-\beta E) & (E<E_2)\end{cases}$$

corresponding to the basin depicted in Fig. 3(a). From the continuity requirements of the steady state flow and of the probability density at the energy thresholds E_1 and E_2 we obtain

$$A_1 = A_2 = A_3 = A,$$

$$B_2 = B_1 + A\int_0^{E_1} \frac{\exp(\beta E)}{\mu_1(E)}\,dE,$$

$$B_3 = B_2 + A\int_{E_1}^{E_2} \frac{\exp(\beta E)}{\mu_2(E)}\,dE.$$

Imposing the condition $p_{ss}(E)\to 0$ for $E\to\infty$ then gives

$$B_3 = -A\int_{E_2}^{\infty} \frac{\exp(\beta E)}{\mu_3(E)}\,dE.$$

All the above constants are replaced in the normalization condition (4.8), which is then used to obtain A

$$A = \beta\Bigg[\int_0^{E_1} \frac{\exp\beta(E-E_1) - \exp\beta E - \exp(-\beta E) + 1}{\mu_1(E)}\,dE + \int_{E_1}^{E_2} \frac{\exp\beta(E-E_2) - \exp\beta E - \exp\beta(E_1-E) + 1}{\mu_2(E)}\,dE + \int_{E_2}^{E_D} \frac{\exp\beta(E-E_D) - \exp\beta E - \exp\beta(E_2-E) + 1}{\mu_3(E)}\,dE + [\exp(-\beta E_D) - 1]\int_{E_D}^{E_\infty} \frac{\exp\beta E}{\mu_3(E)}\,dE\Bigg]^{-1}.$$

The corresponding constants for the landscape depicted in Fig. 3(a) can easily be deduced from the above results by setting $B_2 = B_3$ and $E_1 = E_2 \equiv E_d$.

[1] D. J. Wales, *Energy Landscapes* (Cambridge University Press, Cambridge, 2003).
[2] R. S. Berry and R. Breitengraser-Kunz, Phys. Rev. Lett. **74**, 3951 (1995).
[3] R. E. Kunz and R. S. Berry, J. Chem. Phys. **103**, 1904 (1995).
[4] K. D. Ball, R. S. Berry, R. E. Kunz, F.-Y. Li, A. Proykova, and D. J. Wales, Science **271**, 963 (1996).
[5] O. M. Becker and M. Karplus, J. Chem. Phys. **106**, 1495 (1997).
[6] F. Despa and R. S. Berry, J. Chem. Phys. **115**, 8274 (2001).
[7] N. G. van Kampen, *Stochastic Processes in Physics and Chemistry* (North-Holland, Amsterdam, 1981).
[8] R. E. Kunz, *Dynamics of First-Order Phase Transitions* (Deutsch, Thun, 1995).
[9] A. B. Bortz, M. H. Kalos, and J. L. Leibowitz, J. Comput. Phys. **17**, 10 (1975).
[10] A. F. Voter, Phys. Rev. B **34**, 6819 (1986).
[11] K. A. Fichthorn and W. H. Weinberg, J. Chem. Phys. **95**, 1090 (1991).
[12] D. J. Wales, Mol. Phys. **100**, 3285 (2002).
[13] D. A. Evans and D. J. Wales, J. Chem. Phys. **118**, 3891 (2003).
[14] D. A. Evans and D. J. Wales, J. Chem. Phys. **119**, 9947 (2003).
[15] D. A. Evans and D. J. Wales, J. Chem. Phys. **121**, 1080 (2004).
[16] F. Despa, A. Fernàndez, R. S. Berry, Y. Levy, and J. Jortner, J. Chem. Phys. **118**, 5673 (2003).
[17] F. Despa and R. S. Berry, Eur. Phys. J. D **24**, 203 (2003).
[18] F. Despa and R. S. Berry, J. Chem. Phys. **120**, 5164 (2004).
[19] D. J. Wales, J. P. K. Doye, M. A. Miller, P. N. Mortenson, and T. R. Walsh, Adv. Chem. Phys. **115**, 1 (2000).
[20] J. P. K. Doye and D. J. Wales, Phys. Rev. B **59**, 2292 (1999).
[21] J. P. K. Doye and D. J. Wales, J. Chem. Phys. **111**, 11070 (1999).
[22] J. D. Honeycutt and D. Thirumalai, Proc. Natl. Acad. Sci. U.S.A. **87**, 3526 (1990).
[23] J. D. Honeycutt and D. Thirumalai, Biopolymers **32**, 695 (1992).
[24] M. A. Miller and D. J. Wales, J. Chem. Phys. **111**, 6610 (1999).
[25] K. W. Plaxco and D. Baker, Proc. Natl. Acad. Sci. U.S.A. **95**, 13591 (1998).
[26] J. G. Saven, J. Wang, and P. G. Wolynes, J. Chem. Phys. **101**, 11037 (1994).
[27] R. Zwanzig, J. Chem. Phys. **103**, 9397 (1995).
[28] F. Despa, A. Fernàndez, R. S. Berry, Y. Levy, and J. Jortner, J. Chem. Phys. **118**, 5673 (2003).
[29] R. F. Grote and J. T. Hynes, J. Chem. Phys. **75**, 2191 (1981); **77**, 3736 (1982).
[30] S. A. Adelman, J. Chem. Phys. **64**, 124 (1976).
[31] A. Nitzan, Adv. Chem. Phys. **70**, 489 (1988).
[32] G. H. Weiss, Adv. Chem. Phys. **13**, 1 (1967).
[33] C. A. Angell, Science **267**, 1924 (1995).
[34] C. A. Angell, Prog. Theor. Phys. **126**, 1 (1997).
[35] J. L. Green, K. Ito, K. Xu, and C. A. Angell, J. Phys. Chem. B **103**, 3991 (1999).
[36] F. H. Stillinger, Physica D **107**, 383 (1997).
[37] A. Crisanti, F. Ritort, A. Rocco, and M. Sellitto, J. Chem. Phys. **113**, 10615 (2000).
[38] D. J. Wales and J. P. K. Doye, Phys. Rev. B **63**, 214204 (2001).
[39] F. H. Stillinger and P. G. Debenedetti, J. Chem. Phys. **116**, 3353 (2002).
[40] A. Crisanti and F. Ritort, J. Phys.: Condens. Matter **14**, 1381 (2002).
[41] L. Leuzzi and T. M. Nieuwenhuizen, Phys. Rev. E **64**, 066125 (2001).
[42] D. J. Wales, M. A. Miller, and T. R. Walsh, Nature (London) **394**, 758 (1998).
[43] T. R. Walsh and D. J. Wales, J. Chem. Phys. **109**, 6691 (1998).
[44] M. A. Miller, J. P. K. Doye, and D. J. Wales, Phys. Rev. E **60**, 3701 (1999).
[45] D. G. Lister, J. N. MacDonald, and N. L. Owen, *Internal Rotation and Inversion* (Academic, New York, 1978).
[46] G. M. Zaslavskii and N. N. Filonenko, Sov. Phys. JETP **25**, 851 (1968).
[47] B. Chirikov, Phys. Rep. **C52**, 263 (1979).
[48] M. Abramowitz and I. A. Stegun, *Handbook of Mathematical Functions*, Natl. Bur. Stand. (U.S.) Circ. No. 55 (U.S. GPO, Washington, D.C., 1964).
[49] R. S. Berry, Int. J. Quantum Chem. **58**, 657 (1996).
[50] P. W. Fenimore, H. Frauenfelder, B. H. McMahon, and F. G. Parak, Proc. Natl. Acad. Sci. U.S.A. **99**, 16047 (2002).
[51] F. Despa, D. P. Orgill, J. Newalder, and R. Lee, Burns (to be published).
[52] H. A. Kramers, Physica (The Hague) **7**, 284 (1940).
[53] See, e.g., S. H. Northrup and J. T. Hynes, J. Chem. Phys. **69**, 5246 (1978); **69**, 5261 (1978).
[54] F. Despa, Phys. Status Solidi B **191**, 31 (1995); F. Despa and M. Apostol, Solid State Commun. **94**, 153 (1995); J. Phys. Chem. Solids **57**, 1231 (1996).
[55] J. P. K. Doye and D. J. Wales, J. Chem. Phys. **105**, 8428 (1996).
[56] F. Calvo, F. Spiegelman, and D. J. Wales, J. Chem. Phys. **118**, 8754 (2003).
[57] Y. Levy and O. M. Becker, Phys. Rev. Lett. **81**, 1126 (1998).
[58] O. M. Becker, Y. Levy, and O. Ravitz, J. Phys. Chem. **B104**, 2123 (2000).
[59] Y. Levy, J. Jortner, and O. M. Becker, Proc. Natl. Acad. Sci. U.S.A. **98**, 2188 (2001).
[60] Y. Levy, J. Jortner, and O. M. Becker, J. Chem. Phys. **115**, 10533 (2001).